

## Automated geometry and hexahedral mesh generation for kilometer-scale atmospheric flow simulations

Eero Immonen<sup>1</sup>, Dennis Bengs, Mikael Manngård and Johan Westö

**Summary** This article introduces a methodology for automatic generation of geometries and meshes for kilometer-scale Atmospheric Boundary Layer (ABL) flow simulations, with topography and elevation. The proposed programmatic (hence automatable) *template morphing approach* facilitates interpolation of scattered point cloud terrain data on a template geometry domain, morphing a high-quality quadrilateral template mesh for the interpolated geometry, and setup as well as execution of Computational Fluid Dynamics (CFD) flow simulation. The proposed method specifically addresses the previously reported problems of sustaining an ABL structure across the simulation domain by imposing the velocity and turbulence properties on all vertical surfaces. We present a validation study for the proposed method on an artificial Gaussian hill terrain. A real-world localized wind forecast application from the Turku Archipelago, Finland, is also presented, using open terrain data from National Land Survey of Finland. Such localized wind forecasts aim to assist ships in autonomous navigation and maneuvering in complex port or fairway environments, which is the motivation for this study.

*Key words:* automatic geometry creation, automatic meshing, spatial discretization, Computational Fluid Dynamics, CFD, Atmospheric Boundary Layer, ABL

*Received: 6 June 2022. Accepted: 15 December 2022. Published online: 13 February 2023.*

### Introduction

#### *Background*

The Computational Fluid Dynamics (CFD) simulation process begins by geometry domain creation and spatial discretization, i.e. *meshing*. The geometry creation step must address both the level of detail in 2D or 3D and the spatial extent of modeling, which influence the boundary conditions imposed later in the CFD simulation process. A high-quality mesh, on the other hand, is characterized by a  $y+$  value compatible with the turbulence model, smooth and gradual inter-cell size changes, as well as reasonable skewness, aspect ratio and orthogonal quality metrics. Not only is a high-quality mesh a pre-requisite for accurate and physically realistic results, but it can also facilitate a lower CFD simulation execution time. Vice versa, a poor-quality mesh can result in solver convergence problems and extensive memory use, among others. It is clear that geometry

<sup>1</sup>Corresponding author: [eero.immonen@turkuamk.fi](mailto:eero.immonen@turkuamk.fi)

and mesh creation cannot be treated in isolation of each other in the CFD simulation process.

Many CFD applications today depend on algorithms for *rapid and automatic generation of computational geometries and associated high-quality meshes*. This article is focused on automatic generation of geometries and meshes for kilometer-scale Atmospheric Boundary Layer (ABL) flow simulations, with topography and elevation. The objective is to devise a simulation method, which, based on given terrain geometry point cloud data and mesoscale meteorology, can rapidly produce an accurate localized wind forecast for the geometry domain. Building on the first author’s earlier work on free surface flow simulations [16], we propose a template morphing approach for automatic geometry and CFD mesh generation that facilitates the following items *programmatically*:

- Interpolation of scattered point cloud terrain data on a template geometry domain, with a controlled level of spatial detail and resolution;
- Morphing of a high-quality quadrilateral template mesh for the interpolated geometry, displaying a refined mesh zone at the Region-of-Interest<sup>2</sup> (RoI) and controlled vertical edge growth rate for a given  $y+$  value target.
- Changing wind flow direction and atmospheric boundary layer composition (velocity components and turbulence) at the boundary conditions, while sustaining the ABL structure throughout the fluid domain.

We validate the proposed method on the widely studied Gaussian hill geometry [1, 6, 23], and we illustrate the proposed method in practice by resolving CFD-based localized wind forecasts for the Turku Archipelago, Finland, using open terrain data from National Land Survey (NLS) of Finland. The main application of those forecasts is in assisting autonomous ship operation in complex port and fairway environments by providing wind load forecasts for the ships (e.g. [18, 21, 24]). However, the proposed automatic geometry and mesh creation method may also be useful for wind farm design (e.g. [9, 11, 13, 5]). Moreover, the proposed methodology may be useful for CFD-based shape optimization applications (e.g. [16, 17]), which typically require automated mesh adaptation to a changing geometry. In particular, morphing the same (template) mesh for different geometries helps ensure that the CFD predictions across the simulation cases are comparable [15].

### *CFD for Atmospheric Boundary Layer flow*

CFD prediction of ABL flow has received considerable attention in the past few decades; see e.g. [9, 24, 14] and the references therein. The most widely adopted modeling approach in this context is to place the RoI (say wind farm site) near the bottom center of a large, kilometer-scale, rectangular 3D geometry domain. The classical Monin-Obukhov similarity theory (see [7] and the references therein) coupled with the Richards-Hoxey theory [25] can then be used for implementing the ABL state — i.e., a logarithmic wind profile and turbulence quantities — at CFD simulation boundary conditions.

There are two notable issues with this approach, however. First, as reported by Hargreaves and Wright [14], the Richards–Hoxey theory requires a substantial modification for *sustaining* a neutral ABL even in a simple *empty* rectangular fetch. Second, CFD

<sup>2</sup>In the present work, Region-of-Interest is loosely defined as that circular geometry area where accurate wind forecasts are required. Here, the full geometry domain extends beyond the Region-of-Interest circle, but with limited simulation accuracy due to larger cell sizes.

practitioners always attempt to minimize the simulation time, typically through simulation automation and batch operation of the solution process. For the standard CFD ABL simulations in rectangular domains, described above, this is challenging because even a small change in wind direction requires remeshing as the rectangular geometry boundaries must be realigned to the new wind conditions. This is often tedious manual work, though, over the course of years, methods for automatic mesh generation for ABL simulations have also been proposed in the academic literature; see e.g. [8, 4, 5, 13] and the references therein. Recently, Gargallo-Peiró et al. [12] proposed an automated hybrid meshing strategy (featuring prisms and tetrahedra) for terrain geometries extending to tens of kilometers. However, also in their work, the remeshing procedure has to be invoked for all wind directions.

This article takes a slightly different approach in that a pre-made high-quality quadrilateral template mesh, with pre-designed terrain resolution, is deformed to match the local Earth surface elevation profile. Contrary to the typical rectangular domain approach, in the present work we propose to carry out the CFD simulation in a cylindrical domain, whereby the ABL composition is enforced at both upstream and downstream boundaries from RoI. The demonstration CFD simulations presented in this article show that this helps sustain the ABL structure throughout the domain, without the Hargreaves–Wright modifications [14]. Moreover, the cylindrical flow arrangement facilitates changing wind direction by a simple rotation of the mesh, without remeshing. This feature is especially relevant for practical CFD simulations. On the other hand, at present, the proposed mesh morphing method does not include any post-processing (e.g. Laplacian smoothing), which may be necessary for addressing objects with sharp corners such as tall buildings [16]. Hence the proposed methodology is presently best suited for terrains with smooth elevation changes. Further, we emphasize that the proposed method does not address the many challenges in construction of a meaningful point cloud representation for complex terrains (such as removal of trees).

## Methodology

### *Digital elevation model*

The geometry creation process utilized herein is based on the Digital Elevation Model (DEM) (see e.g. [20, 26, 22] and the references therein). It is a numerical representation of the Earth’s surface that contains height points representing the topography. DEM elevations represent bare earth, without vegetation and buildings, but may include other manmade features, such as road embankments [20]. Typically, country-wide DEMs are produced by using airborne laser scanning, and are stored in a data system as a regular grid or a triangulated irregular network. In this study, we utilized the elevation model 2 m (DEM2), which depicts the height of the terrain above sea level, according to the specification N2000 height (EPSG:3900). It is the most accurate elevation model of Finland [19]. The DEM2 triangulation yields a point cloud  $(x, y, z)$  representation for the geometry domain.

### *Scattered data interpolation*

The ground elevation is assumed, by suitable translation and rotation, to be described by a set of  $(x, y, z)$  coordinate points, such that the vertical elevation is in  $y$  direction and sea level is at  $y = 0$ . For simulation model creation, a rectangular domain is extracted

from the point cloud data, with the RoI centroid at the origin  $(0, 0, 0)$ . At this step, one specifies the radius of the circular region for CFD simulations, bearing in mind that the CFD simulation results are the most accurate in the vicinity of the RoI, and less so near the vertical boundary. Figure 6 illustrates this approach. The point cloud is associated with a scattered data interpolation function  $F : \mathbb{R}^2 \rightarrow \mathbb{R} : (x, z) \rightarrow F(x, z)$  that is used for representing the ground surface elevation across the circular region [2].

### *Template geometry and mesh*

The template geometry is a cylindrical domain with the sector-like structure (for controlled meshing) displayed in Figure 1. Its primary axis is aligned with the vertical ( $y$ ) axis and the origin coincides with the point cloud RoI centroid. The vertical extent of the domain should be large enough to represent the atmospheric boundary layer velocity profile, such that the artificial boundary at the top only minimally influences the flow near the ground.

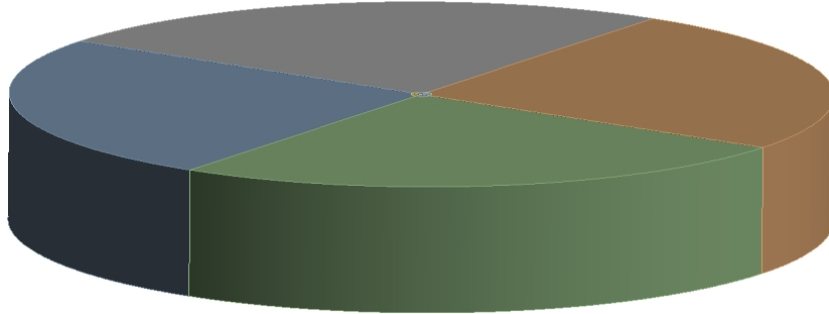


Figure 1. An example of a template geometry.

The template mesh consists of quadrilateral elements, with a structured section away from the RoI and an unstructured section near the RoI. The proposed mesh construction aims to ensure good accuracy near the RoI, and a low cell count away from it. The mesh grows radially from the primary ( $y$ ) axis in the structured mesh zone and vertically from the bottom ( $y = 0$ ) everywhere. The vertical edge sizing can be controlled later during mesh morphing, but the edge and face sizing on the  $y = 0$  plane surface should be chosen according to the required terrain representation accuracy.

The above aspects are illustrated in Figure 2, which we used as the template mesh for the demonstration simulations reported later in this article (see Figure 7). This template mesh covers 2 km diameter ( $xz$ ) and 200 m height ( $y$ ) in 3.6 million cells. Near the RoI, the minimum grid edge length in the  $xz$  plane is approximately 0.1 m, and towards the wind inlet boundaries grows to up to 30 m. The vertical span is covered by 60 layers, with the first mesh layer at 0.05 m above the ground surface boundary.

### *Interpolation and mesh morphing*

The interpolation and mesh morphing procedure is described in Algorithm 1. In the present work, it was implemented in Matlab R2019b to process ASCII format ANSYS Fluent mesh files (extension .msh) described in the software documentation [3]. For a template mesh of 3.6 million cells (Figure 1) and a cloud size of 50000  $(x, y, z)$  points, the algorithm execution took approximately 45 minutes on a desktop workstation. The algorithm has not been optimized for speed.

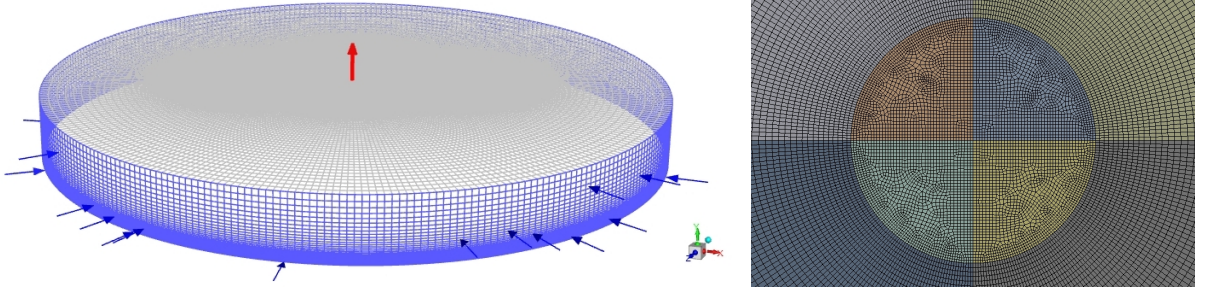


Figure 2. Left: An example of a hexahedral template mesh for a cylindrical geometry (3.6M cells). Right: View along the  $y$ -axis shows an unstructured mesh near the RoI and a structured mesh away from it.

---

**Algorithm 1** Template mesh morphing by ground surface elevation function  $F$

---

**Require:** Template mesh  $\mathcal{M}$ , with nodes  $\mathcal{N}$

**Require:** Monotonically increasing scaling function  $f_y : [0, 1] \rightarrow [0, 1]$ , with  $f_y(0) = 0$  and  $f_y(1) = 1$

**Require:** Scattered data interpolation function  $F$

- 1:  $d_{max} \leftarrow \max \{n_y \mid \mathbf{n} = (n_x, n_y, n_z) \in \mathcal{N}\}$  ▷ Height of template domain
  - 2:  $\mathcal{N}_g \leftarrow \{\mathbf{m} = (m_x, m_y, m_z) \in \mathcal{N} \mid m_y = 0\}$  ▷ Find ground nodes
  - 3:  $\mathcal{D}(\mathbf{m}) \leftarrow \{\mathbf{n} = (n_x, n_y, n_z) \in \mathcal{N} \setminus \mathcal{N}_g \mid \mathbf{m} \in \mathcal{N}_g, n_x = m_x, n_z = m_z\}$  ▷ Vertically aligned with  $\mathbf{m}$
  - 4: **for**  $\mathbf{m} = (m_x, m_y, m_z) \in \mathcal{N}_g$  **do**
  - 5:      $y_{new}^m \leftarrow F(m_x, m_z)$  ▷ Interpolate
  - 6:      $\mathbf{m} \leftarrow (m_x, y_{new}^m, m_z)$  ▷ Move ground node  $\mathbf{m}$
  - 7:      $d_{new} = d_{max} - y_{new}^m$  ▷ Adjust height by deformation
  - 8:     **for**  $\mathbf{n} = (n_x, n_y, n_z) \in \mathcal{D}(\mathbf{m})$  **do**
  - 9:          $r \leftarrow f_y(n_y/d_{max})$  ▷  $r \in [0, 1]$
  - 10:          $y_{new}^n \leftarrow y_{new}^m + d_{new} \cdot r$  ▷  $y_{new}^n \in (y_{new}^m, d_{max}]$
  - 11:          $\mathbf{n} \leftarrow (n_x, y_{new}^n, n_z)$  ▷ Move vertically aligned nodes in  $\mathcal{D}(\mathbf{m})$
  - 12:     **end for**
  - 13: **end for**
- 

We emphasize that the vertical growth of cell sizes (e.g. for  $y+$  matching) can be controlled at line 9 in Algorithm 1. The trivial scaling function choice  $x \rightarrow f_y(x) = x$ , also used in the numerical simulations presented in this article, yields the same cell size scaling ratio as in the template mesh.

### *Simulation boundary conditions*

Similar to [14, 24], we propose to utilize the  $k$ - $\epsilon$  turbulence specification with a modified turbulent Prandtl number  $\sigma_\epsilon = 1.11$  corresponding to the Von Kármán constant  $\kappa = 0.4$ . For a given friction velocity  $u_*$ , we can define the  $x$ -velocity ( $u$ ) and the turbulence model

quantities  $k$ ,  $\epsilon$  at any height  $y$  on the boundary as follows:

$$u = u(y) = \frac{u_*}{\kappa} \ln \left( \frac{y + y_0}{y_0} \right) \quad (1)$$

$$k = k(y) = \frac{u_*^2}{\sqrt{C_\mu}} \quad (2)$$

$$\epsilon = \epsilon(y) = \frac{u_*^3}{\kappa(y + y_0)} \quad (3)$$

Here  $C_\mu = 0.09$  (from  $k$ - $\epsilon$  theory), and  $y_0$  is the surface roughness length, chosen according to the terrain composition [27]. In this approach, the friction velocity  $u_*$  is calibrated to yield a given reference wind speed at a fixed reference height (e.g.  $u(y) = 8 \frac{\text{m}}{\text{s}}$  at  $y = 6 \text{ m}$  as in the demonstration simulations reported later in this article), and only the reference wind speed is to be varied in simulations. A comparison to the standard  $k$ - $\omega$  SST turbulence specification is reported in the next section for reference.

For CFD simulation boundary conditions, the quantities (1)–(3) are to be implemented on the circular velocity inlet surface (denoted in blue in Figure 1). The ground surface is a no-slip wall with roughness height  $\epsilon_r = 20 \cdot y_0$ , as suggested by Hargreaves and Wright [14]. The flat top section (denoted in gray in Figure 1) is a zero shear wall, with a small pressure outlet patch (denoted in red in Figure 1) specified at 0 Pa.

### Validation: Gaussian hill geometry

To validate the proposed methodology, we studied wind flow over the Gaussian hill geometry [1, 6, 23]. It is an infinitely smooth isolated hill surface defined by the equation:

$$y = h e^{-\frac{1}{2} \left( \frac{r}{\sigma} \right)^2}, \quad \text{with } r = \sqrt{x^2 + z^2} \quad (4)$$

Two validation studies were carried out. The first validation study aimed to assess the sensitivity of the CFD predictions to fluid domain shape, choice of the simulation model, and grid structure as well as its resolution. The second validation study involved a comparison of the CFD predictions obtained by the proposed methodology to those reported in the literature. For additional robustness, we utilized slightly different Gaussian hill geometries in the two validation studies.

#### *First validation: Sensitivity to geometry, mesh and simulation model parameters*

The parameters of the Gaussian hill surface in this first validation study were chosen as  $h = 700 \text{ m}$ ,  $\sigma = 986.5 \text{ m}$ . The cylindrical template geometry utilized herein has a diameter of 20 km, and it extends vertically up to 5 km. A coarse resolution mesh of 110k cells (Figure 3, Left) and a fine resolution mesh of 1.29M cells (not shown) were implemented on the geometry based on the proposed template morphing method. For CFD simulations, the following ABL structure proposed by Ravensbergen et al. [23] was adopted:

$$u(y) = U_{ref} \frac{u_*}{\kappa} \ln \left( \frac{y}{y_0} \right) \quad (5)$$

with  $y_0 = 2.29 \cdot 10^{-7} \text{ m}$ ,  $\kappa = 0.41$ ,  $U_{ref} = 10.9 \frac{\text{m}}{\text{s}}$  and  $u_* = 0.0191$ . This ABL specification ensures a flow velocity of  $U_{90m} = 10 \frac{\text{m}}{\text{s}}$  at 90 m height, a condition arising from wind farm design concerns. Both the  $k$ - $\epsilon$  turbulence model (2)–(3), and the standard  $k$ - $\omega$  SST

turbulence model, at 5% turbulent intensity at the inlet surface (as suggested in [6], p. 92, for this ground surface roughness  $y_0$ ), were utilized in the CFD simulations.

For comparison, a rectangular geometry, extending between  $-10 \dots 10$  km in the  $xz$ -plane, and between  $0 \dots 5$  km in the  $y$  direction, was also implemented for the above Gaussian hill. A polyhedral mesh, with a 10-cell prismatic boundary layer and 303k cells, was generated in ANSYS Fluent 2021R2 (Figure 3, Right). The wind flow is in the  $+x$  direction. For the rectangular domain, the ABL velocity profile (5) was only specified at the inlet, and the opposing flow discharge surface was specified as a pressure outlet at 0 Pa (gauge). The other flat surfaces were specified as zero shear walls. The considered turbulence models were the same as for the cylindrical geometry.

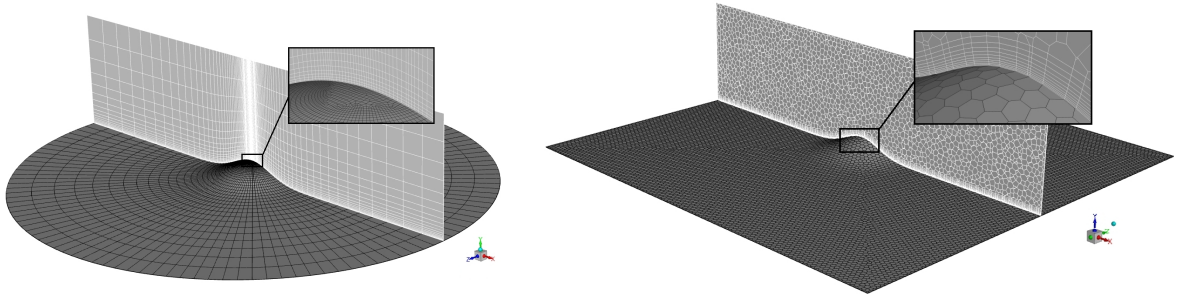


Figure 3. Left: Deformed coarse template mesh (110k cells), with  $xy$  plane shown. Right: Rectangular grid with polyhedral elements (303k cells), with  $xy$  plane shown.

ANSYS Fluent 2021R2 was utilized for resolving the Reynolds-Averaged Navier–Stokes (RANS) equations in double precision arithmetic, for ideal gas air. Figure 4 displays the CFD prediction of wind velocity magnitude at 90 m height in the  $y$ -direction from the ground surface on the  $xy$ -plane. Both velocity and  $x$ -coordinate are normalized as in [6, 23]. It is clear from Figure 4 that the proposed method produces CFD results that are not sensitive to the parameters considered herein. The biggest differences across the simulated cases are seen at  $x \approx 3h$  downstream from the hill, which is likely attributed to differences in predicted flow separation and reattachment patterns.

### *Second validation: Comparison to known results*

The second validation study involved a comparison to known results reported in the literature. The reference case was obtained from Ravensbergen et al. [23] and Barthelmie et al. [6] who carried out wind flow simulations for a Gaussian hill with  $h = 700$  m (as in the first validation study) and  $\sigma = 1486$  m, making the bump more shallow than in the first validation study reported above. We utilized the two template meshes (coarse at 110k cells and fine at 1.29M cells) from first validation study, with linear scaling in the  $xz$ -plane. The diameter of the geometry was 25 km, and height 5 km, making it comparable to the one utilized by Ravensbergen et al. [23]. The wind flow conditions in the second validation study were the same as in the first one, based on the  $k - \epsilon$  turbulence model (2)–(3). The simulation environment was also identical to that in the first validation study.

Figure 5 displays the CFD prediction of normalized wind velocity magnitude at 90 m height ( $y$ -direction) from the ground surface. Clearly the CFD predictions, utilizing the proposed methodology on the cylindrical domain with fine mesh at 1.29M cells, coincide

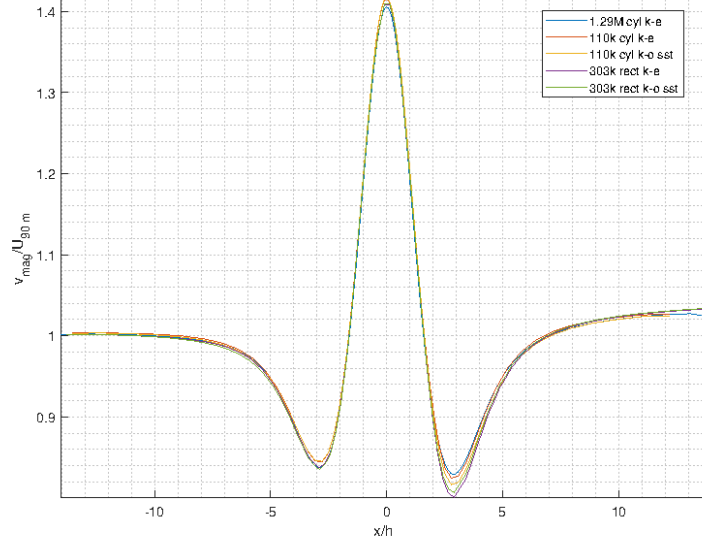


Figure 4. Sensitivity to geometry (cylindrical, rectangular), mesh (110k, 303k, 1.29M cells) and simulation model ( $k - \epsilon$ ,  $k - \omega$  SST) parameters, for a Gaussian hill geometry.

well with those reported by Ravensbergen et al. [23]. Figure 5 also displays the degree of variation that can be expected in the CFD prediction results in practice. We emphasize, in particular, that the largest variation occurs right downstream from the hill — similar to Figure 4.

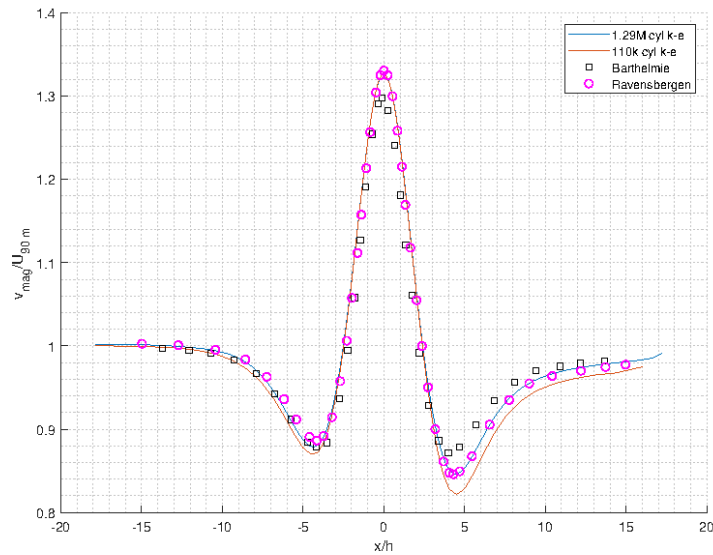


Figure 5. Comparison to previously reported data in Ravensbergen et al. [23] and Barthelmie et al. [6], for a Gaussian hill geometry.

### Practical application: Localized wind forecasts for the Turku archipelago

In this section, we demonstrate the proposed simulation methodology for a geometry domain in the Turku archipelago, Finland. Altogether 24 simulation cases were resolved,

corresponding to 8 wind directions and 3 wind speeds, in a batch simulation on the Puhti supercomputer at CSC — IT Center for Science, Finland. For brevity, here we only report simulation results for one wind direction and reference speed.

### Geometry and mesh

The RoI centroid is at entrance to Turku port ( $60^{\circ}25'19.2''\text{N}$   $22^{\circ}09'40.0''\text{E}$ ), as shown together with the area DEM representation in Figure 6. We assume that the fairway extends  $\pm 100$  m around the centroid, resulting in a 200 m RoI with higher resolution. Morphing the template mesh shown in Figure 1 yields the terrain surface representation and computational mesh shown in Figure 7.

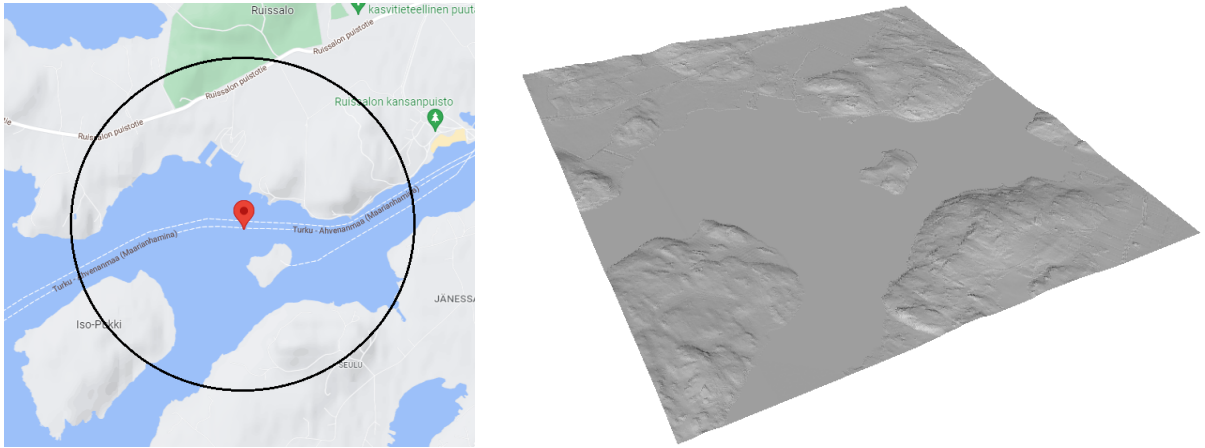


Figure 6. Left: Map layout at entrance to Turku port ( $60^{\circ}25'19.2''\text{N}$   $22^{\circ}09'40.0''\text{E}$ ), with the RoI centroid (origin) highlighted in red and the extent of CFD modeling depicted in black. Right: Corresponding DEM representation.

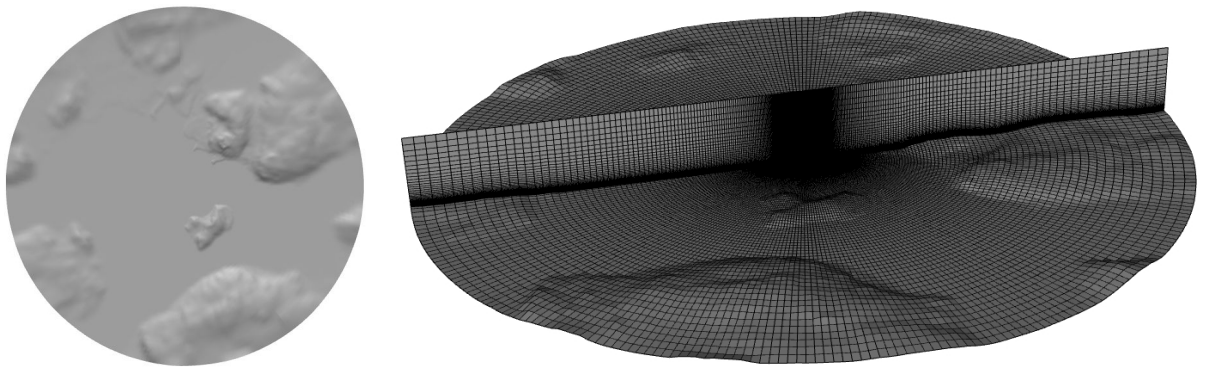


Figure 7. Left: Terrain surface on the deformed template (the RoI is at centroid where also the spatial resolution is the highest). Right: Parts of the computational mesh, with highest resolution near the RoI.

### CFD simulations

The reference speed was chosen at  $u(y) = 8 \frac{\text{m}}{\text{s}}$  at  $y = 6$  m, and the desired wind direction was obtained by rotating the deformed mesh  $90^{\circ}$  about the principal axis. The surface

roughness length was set at  $y_0 = 0.01$  as a compromise between recommendation for open sea ( $y_0 = 0.0002$ ) and occasional large obstacles ( $y_0 = 0.1$ ). This value is in accordance with the experimental findings of Colin and Faivre [10], and it is the same as used by Hargreaves and Wright [14].

The quantities (1)–(3) were implemented as User-Defined Functions (UDF) into ANSYS Fluent 2021R2. The RANS equations were then resolved in double precision arithmetic, for ideal gas air. The total simulation time on 40 cores on the Puhti supercomputer at CSC was approximately 2.5 hours over 2000 iterations, which was experimentally found to be sufficient for numerical convergence for all wind directions and speeds considered in this study.

### Simulation results

Figure 8 and Figure 9 display the localized wind forecast near the RoI. Clearly the ABL structure can be maintained throughout the simulation domain, and the terrain elevations have a significant effect on the local wind conditions in the fairway.

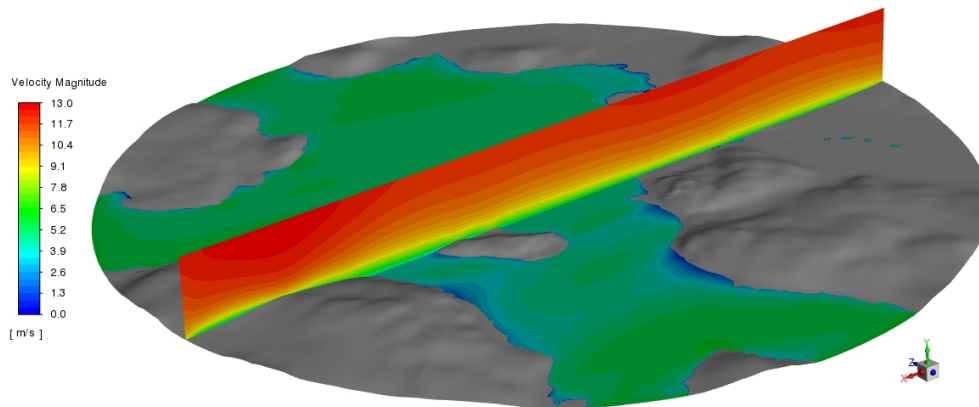


Figure 8. CFD predictions of wind velocity magnitude at  $xy$  plane and at  $y = 1$  m. Wind is  $8 \frac{\text{m}}{\text{s}}$  at  $y = 6$  m height, flowing in the  $+x$  direction (i.e. parallel to the shown  $xy$  plane).

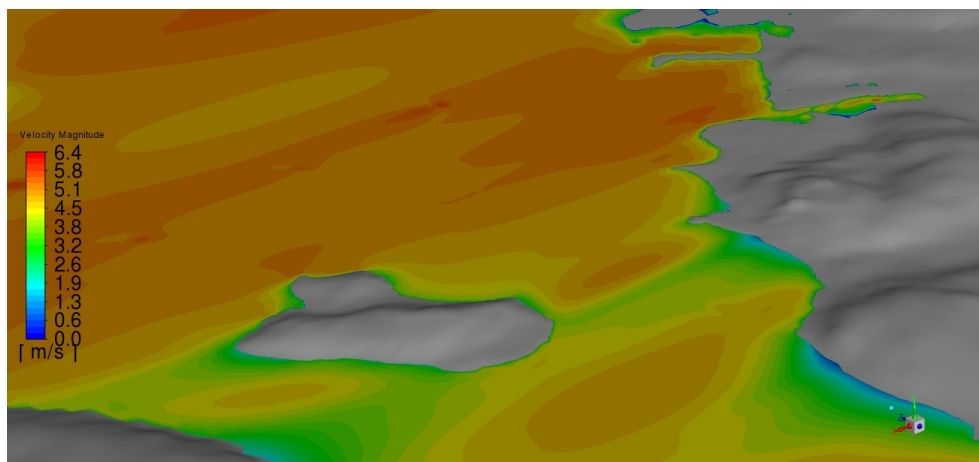


Figure 9. Closeup of CFD predictions of wind velocity magnitude at  $y = 1$  m near the origin. Wind conditions are as in Figure 8.

## Conclusions and future work

We have introduced a method for automatic generation of geometries and meshes for kilometer-scale atmospheric flow simulations, based on digital elevation terrain models. The proposed programmatic template morphing approach facilitates interpolation of scattered point cloud terrain data on a template geometry domain, morphing a high-quality quadrilateral template mesh for the interpolated geometry, and batch execution of CFD flow simulations. The resolution of the terrain topography for CFD simulations is specified in the template mesh, whereas the vertical resolution (e.g. for  $y+$  matching) can be programmatically controlled during mesh morphing. In this article, the proposed method has been validated on the widely studied Gaussian hill geometry and illustrated in practice for generating localized CFD-based wind forecasts for the Turku Archipelago, Finland.

Future work on the topic should focus on mesh smoothing during morphing to address abrupt large changes in vertical elevation (such as tall buildings). Moreover, the simulation methodology should be adapted for spatially varying surface roughness values instead of a single constant value utilized here. The execution speed of Algorithm 1 could potentially be significantly reduced by optimization in a future study. Finally, experimental validation studies should be carried out to assess the numerical accuracy of the proposed methodology, especially in comparison to the many methods utilized in wind farm design.

## Acknowledgements

The authors would like to thank the anonymous reviewers for several suggestions for improving the article. Research project funding from Ministry of Culture and Education is gratefully acknowledged (ARPA — Applied Research Platform for Autonomous Systems).

## References

- [1] ABDI, D. S., AND BITSUAMLAK, G. T. Wind flow simulations on idealized and real complex terrain using various turbulence models. *Advances in Engineering Software* 75 (2014), 30–41. <https://doi.org/10.1016/j.advengsoft.2014.05.002>.
- [2] AMIDROR, I. Scattered data interpolation methods for electronic imaging systems: A survey. *Journal of electronic imaging* 11, 2 (2002), 157–176. <https://doi.org/10.1117/1.1455013>.
- [3] ANSYS, INC. Fluent and tgrid mesh file format. <https://romeo.univ-reims.fr/documents/fluent/tgrid/ug/appb.pdf>. Accessed: 2022-03-31.
- [4] AVILA, M., FOLCH, A., HOUZEAUX, G., EGUZKITZA, B., PRIETO, L., AND CABEZÓN, D. A parallel CFD model for wind farms. *Procedia Computer Science* 18 (2013), 2157–2166. <https://doi.org/10.1016/j.procs.2013.05.386>.
- [5] AVILA, M., GARGALLO-PEIRÓ, A., AND FOLCH, A. A CFD framework for offshore and onshore wind farm simulation. In *Journal of Physics: Conference Series* (2017), vol. 854, IOP Publishing, pp. 012002. <https://doi.org/10.1088/1742-6596/854/1/012002>.
- [6] BARTHELMIE, R. J., FRANSEN, S. T., RATHMANN, O., HANSEN, K., POLITIS, E., PROSPATHOPOULOS, J., SCHEPERS, J., RADOS, K., CABEZÓN, D., SCHLEZ,

- W., ET AL. Wind flow simulations on idealized and real complex terrain using various turbulence models. Tech. Rep. R-1765(EN), Risø DTU, 2011. <https://www.osti.gov/etdeweb/servlets/purl/1016226>, Accessed: 2022-05-27.
- [7] BREEDT, H. J., CRAIG, K. J., AND JOTHIPRAKASAM, V. D. Monin-Obukhov similarity theory and its application to wind flow modelling over complex terrain. *Journal of Wind Engineering and Industrial Aerodynamics* 182 (2018), 308–321. <https://doi.org/10.1016/j.jweia.2018.09.026>.
- [8] CANIOT, G., LI, W., AND DUPONT, G. Validations and applications of a CFD tool dedicated to wind assessment in urban areas. In *13th International Conference on Wind Engineering* (2011).
- [9] CHAUDHARI, A. *Large-eddy simulation of wind flows over complex terrains for wind energy applications*. PhD thesis, Lappeenranta University of Technology, 2014.
- [10] COLIN, J., AND FAIVRE, R. Aerodynamic roughness length estimation from very high-resolution imaging LIDAR observations over the Heihe basin in China. *Hydrology and Earth System Sciences* 14, 12 (2010), 2661–2669. <https://doi.org/10.5194/hess-14-2661-2010>.
- [11] FANG, H.-F. Wind energy potential assessment for the offshore areas of Taiwan west coast and Penghu Archipelago. *Renewable Energy* 67 (2014), 237–241. <https://doi.org/10.1016/j.renene.2013.11.047>.
- [12] GARGALLO-PEIRÓ, A., AVILA, M., AND FOLCH, A. A hybrid meshing framework adapted to the topography to simulate atmospheric boundary layer flows. *Computer-Aided Design* 144 (2022), 103168. <https://doi.org/10.1016/j.cad.2021.103168>.
- [13] GARGALLO-PEIRÓ, A., AVILA, M., OWEN, H., PRIETO, L., AND FOLCH, A. Mesh generation for atmospheric boundary layer simulation in wind farm design and management. *Procedia Engineering* 124 (2015), 239–251. <https://doi.org/10.1016/j.proeng.2015.10.136>.
- [14] HARGREAVES, D., AND WRIGHT, N. G. On the use of the  $k-\varepsilon$  model in commercial CFD software to model the neutral atmospheric boundary layer. *Journal of wind engineering and industrial aerodynamics* 95, 5 (2007), 355–369. <https://doi.org/10.1016/j.jweia.2006.08.002>.
- [15] IMMONEN, E. Shape optimization of annular s-ducts by CFD and high-order polynomial response surfaces. *Engineering Computations* 35, 2 (2018), 932–954. <https://doi.org/10.1108/EC-08-2017-0327>.
- [16] IMMONEN, E. A parametric morphing method for generating structured meshes for marine free surface flow applications with plane symmetry. *Journal of Computational Design and Engineering* 6, 3 (2019), 348–353. <https://doi.org/10.1016/j.jcde.2018.11.002>.
- [17] IMMONEN, E. Optimal design for disc golf by computational fluid dynamics and machine learning. *Structural and Multidisciplinary Optimization* 65, 1 (2022), 1–17. <https://doi.org/10.1007/s00158-022-03177-1>.

- [18] JANSSEN, W., BLOCKEN, B., AND VAN WIJHE, H. CFD simulations of wind loads on a container ship: Validation and impact of geometrical simplifications. *Journal of wind engineering and industrial aerodynamics* 166 (2017), 106–116. <https://doi.org/10.1016/j.jweia.2017.03.015>.
- [19] NLS - NATIONAL LAND SURVEY OF FINLAND. Digital elevation model. <https://www.maanmittauslaitos.fi/en/research/interesting-topics/digital-elevation-model>. Accessed: 2022-04-04.
- [20] OKSANEN, J. *Digital elevation model error in terrain analysis*. PhD thesis, University of Helsinki, 2006.
- [21] PAWELSKI, J., PIOTRZKOWSKI, W., ŚNIEGOCKI, H., AND WILCZYŃSKI, P. Factors affecting safety of handling ultra large container vessels in Port of Gdańsk. *Autobusy: technika, eksploatacja, systemy transportowe* 20 (2019), 313–316. <https://doi.org/10.24136/atest.2019.057>.
- [22] POLIDORI, L., AND EL HAGE, M. Digital elevation model quality assessment methods: A critical review. *Remote Sensing* 12, 21 (2020), 3522. <https://doi.org/10.3390/rs12213522>.
- [23] RAVENSBERGEN, M., HELGEDAGSRUD, T. A., BAZILEVS, Y., AND KOROBENKO, A. A variational multiscale framework for atmospheric turbulent flows over complex environmental terrains. *Computer Methods in Applied Mechanics and Engineering* 368 (2020), 113182. <https://doi.org/10.1016/j.cma.2020.113182>.
- [24] RICCI, A., JANSSEN, W., VAN WIJHE, H., AND BLOCKEN, B. CFD simulation of wind forces on ships in ports: Case study for the Rotterdam Cruise Terminal. *Journal of Wind Engineering and Industrial Aerodynamics* 205 (2020), 104315. <https://doi.org/10.1016/j.jweia.2020.104315>.
- [25] RICHARDS, P., AND HOXEY, R. Appropriate boundary conditions for computational wind engineering models using the  $k-\varepsilon$  turbulence model. *Journal of wind engineering and industrial aerodynamics* 46 (1993), 145–153. [https://doi.org/10.1016/0167-6105\(93\)90124-7](https://doi.org/10.1016/0167-6105(93)90124-7).
- [26] SEIJMONSBERGEN, A. C., HENGL, T., AND ANDERS, N. S. Semi-automated identification and extraction of geomorphological features using digital elevation data. In *Developments in Earth Surface Processes*, vol. 15. Elsevier, 2011, pp. 297–335. <https://doi.org/10.1016/B978-0-444-53446-0.00010-0>.
- [27] WMO. Guide to meteorological instruments and methods of observation. *Geneva, Switzerland* (1996).

Eero Immonen  
 Computational Engineering and Analysis Research Group  
 Turku University of Applied Sciences  
 ICT-City, Joukahaisenkatu 3, 20520 Turku, Finland  
 eero.immonen@turkuamk.fi

Dennis Bengs  
 Novia University of Applied Sciences

Wolffskavägen 33, 65200 Vasa, Finland  
dennis.bengs@novia.fi

Mikael Manngård, Johan Westö  
Faculty of Technology and Seafaring  
Novia University of Applied Sciences  
Aboa Mare, Auriga Business Center, Juhana Herttuan puistokatu 21, 20100 Turku, Finland  
mikael.manngard@novia.fi, johan.westo@novia.fi